Structural, Optical & Dielectric Behavioural Analysis of Nb_2O_5-V_2O_5 Modified Barium-Boro-Bismuthate Glasses: Opto-Electronic Applications

Vikas Attri[1], M.S. Dahiya[1,2], Ashima Hooda[1], A. Agarwal[3] and Satish Khasa[1]*

[1] Department of Physics, Deenbandhu Chhotu Ram University of Science and Technology, Murthal, Haryana, India
[2] Directorate of Education, Govt. of NCT, Delhi
[3] Department of Physics, Guru Gambheswer University of Science and Technology, Hisar, Haryana, India

Volume 1, Issue 4, July 2024
Received:28 April, 2024; Accepted: 12 July, 2024
DOI: https://doi.org/10.63015/5C-2428.1.4

* *Corresponding Author Email: skhasa.phy@dcrustm.org*

Abstract: Barium-Boro-Bismuthate glasses modified with Nb_2O_5 and V_2O_5 having composition $x$$Nb_2O_5$-(10-$x$)$V_2O_5$-25BaO-30$B_2O_3-35Bi_2O_3$ (where x = 0, 1, 3, 5, 8, 9 and 10 mol%) were prepared via melt-quench technique and investigated for structural, optical, electrical and thermal properties. The produced glasses were subjected to thermal exposure for five hours at 450 °C in order to examine structural modifications inside the glass matrix. Densities of as-prepared glass samples were measured and values were found to lie in order of 5.5 g/cc. XRD profile containing broad humps for as-prepared glass samples reflected their amorphous nature, and ordered peak pattern for annealed glass samples reflected development of $Bi_{45}BO_{69}$ crystalline phase (with crystallite size < 50 nm) inside annealed glass matrix. FTIR spectroscopy helps in identification of different structural units (such as BO_4, BO_3, BiO_6 & BiO_3) inside base glass matrix. Dielectric analysis reflects usability of glass samples for high frequency signal transmission, high-temperature semi-conducting and energy storage devices. Lower value for ac conductivity (~10^{-5} S/m) reflects usability of glass samples towards high-voltage bearing materials (due to high resistance for electrical breakdown). Optical band-gaps (E_g) for as-prepared and annealed glass samples lie between 1.13 and 2.39 eV, suggesting their usability towards various optical and opto-electronic devices (such as absorber material in solar cells, optical fibre, lenses, filters, etc.). A non-significant change in refractive index values for as-prepared glass samples after annealing reflected enlisted these into transparent glass ceramic category. A single sharp exothermic peak in each differential thermal analysis (DTA) curve reflects nucleating ability of as-prepared glass samples.

Keywords: Nano-crystallites, optical band-gap, refractive indices, ac conductivity, differential thermal analysis, transparent glass ceramics, mixed transition metal effect

1. Introduction: The demand for low-cost, sustainable, chemically robust, and dependable materials for optoelectronic devices is rising quickly. Consequently, enormous research efforts have been made by scientists all over the world to create novel materials that fulfil these specifications. Researchers have focused especially on oxide glasses (including borate, vanadate, bismuthate, and tellurite) imparting transition metals due to their usability in optoelectronic devices. These glasses can be prepared in order to target a particular application or behaviour, such as insulation, conduction, optical transparency, low melting point, waveguide, water resistance, etc. [1–5]. Boro-bismuthate glass network mainly contains three and four coordinated borate units (i.e. BO_3 and BO_4) along with three and six coordinated bismuthate units (i.e. BiO_3 and BiO_6). Modification of glass matrix with alkali oxides or alkali earth oxides (like BaO, Li_2O, etc.) in boro-bismuthate glass network endows their physical, optical, thermal and electrical properties by defining the glass matrix [6–8].

The presence of transition metal ions (TMIs) in glass matrix causes enhancements in thermal and spectroscopic properties due to polaronic conductions, local order or disorder in glass matrix and hoping of charge carriers [9]. TMI's such as Nb, Fe, V, Co, etc. were coordinated with non-bridging oxygen (i.e. compensating the extra charge and found to form some extrinsic dipoles to form a trap type entity where the charge carriers (electrons and holes) will be trapped and dipole polarization will occur inside the glass matrix [9–11]. The existence of TMIs in multiple oxidation states makes these materials (glass or glass-ceramics) useful for applications like UV irradiation shielding windows and glass lasers. These ions can mainly act as network modifiers or formers helping to tailor electrical, optical, and thermal properties of glasses [12–14].

Glasses containing Nb_2O_5 can be treated as usable materials for piezoelectric, semi-conducting and radiation shielding materials with high stimulated emission parameters [13]. The addition of V_2O_5 and Nb_2O_5 causes enhancements in optical and thermal behaviour of boro-bismuthate glass matrix [15–19]. With all these enhancements, these oxides (or ions) also intensify the crystallization abilities of glass matrix [1,20]. Alongside the investigation of the borate network, the spectroscopic futures of Nb_2O_5 placed into the network were also being examined. It was found that borate glasses containing Nb_2O_5 exhibit substantial UV absorption, better transparency in the visible-IR range, enhanced nonlinear optical properties and possess high refractive indices [21]. Moreover, Nb_2O_5 exists in Nb^{4+} and Nb^{5+} oxidation states, which helps to increase electrical conductivity (through polaronic conduction contribution) of glass samples. Boro-bismuthate glasses having niobium metal oxide possess large chemical resistance, high refractive index, high vickers hardness, fair transparency in Vis-IR region [13,16]. A number of researchers tried to investigate structural contribution of Nb_2O_5 in various silicate, germanate and borate glass matrices, as per IR and Raman spectroscopic outcomes [17,22,23]. Majority of these investigations suggest existence of Nb^{5+} ions (i.e. Nb_2O_5 acts as glass formers), which have a significant effect on thermal and opto-electrical properties of glass systems. The addition of Nb_2O_5 increases the crystal field strength, helps for phase separation and helps increase the nucleation ability of glass system [1,13,14,16,25–30,31–34,]. An enhancement in physical, electrical, optical properties, with addition of TMI's has been observed in literature [5,27,34–36]. The dynamics of multi TMIs in barium-boro-bismuthate glass systems may therefore be interesting to investigate. Keeping in mind these facts, the study aims to investigate how the inclusion of Nb_2O_5 at the cost of V_2O_5 affects the optical, electrical and thermal abilities of barium boro-bismuthate glass system.

2 Sample Synthesis and Experimental Techniques

2.1 Glass synthesis

Nb_2O_5-V_2O_5 substituted barium boro-bismuthate glass samples with chemical composition $x$$Nb_2O_5$-(10-$x$)$V_2O_5$-25BaO-30$B_2O_3-35Bi_2O_3$ (where x can take values from 0.0, 1.0, 3.0, 5.0, 8.0, 9.0 and 10.0) were prepared using melt-quench methodology and shortened as NVBBBx (where x = 0, 1, 3, 5, 8, 9 and 10). For synthesis, the AR/GR grade starting raw chemicals (i.e. Bi_2O_3 (HIMEDIA, 99.5%), B_2O_3 (HIMEDIA (ACS grade, 99.8% pure)), BaO (HIMEDIA (ACS grade, 99%)), V_2O_5 and Nb_2O_3 (HIMEDIA (AR grade, 99.5%))) were weighed (as per composition) and mixed (homogenously) through agate pestle mortar. The prepared homogenous mixture was transferred to high alumina crucible and placed in electrical muffle furnace (operating at 1150°C) for an hour with regular shaking in every 15 minutes (in order to keep the melt homogenous). The obtained melt (mixture) was quenched or sandwiched between two preheated SS plates (in order to reduce thermal stress), resulting in glass samples with thickness ranging from 0.5 - 1 mm. Samples were polished and cut into rectangular shapes for dielectric studies. A portion of prepared glass samples was finely powdered for analyzing their optical, structural

and thermal behaviour. As-prepared glass samples were exposed thermally (annealed) at 450 °C for five hours in order to investigate any structural change or crystallite growth inside glass matrix.

2.2 Experimental Techniques

2.2.1 Density measurements

Density measurements (performed at room temperature via Archimedes principle) help to analyze the physical behaviour of sample. Xylene (density of 0.863 g/cc) was used as buoyant liquid (because of its inert nature with glasses). A digital single pen weighing balance (Model- CAS CAUY 220) with a minimum count of 0.1 mg, was used for weight recording. Density measurements and molar volume estimations for each prepared sample were performed as per relation (see equations (i & ii)) [18,37].

$$\rho = \frac{W_a}{W_a - W_x} \times \rho_x \qquad \text{(i)}$$

Here ρ, ρ_x are densities of glass sample and xylene, W_a, W_x are weights of glass sample in air and in xylene respectively. The molar volume (V_m) of prepared samples can be analyzed using molecular mass (M) and density (ρ) via relation given below.

$$V_m = \frac{M}{\rho} \qquad \text{(ii)}$$

2.2.2 X-ray diffraction (XRD) profile

Rigaku Ultima-IV, (X-ray diffractometer) working with Cu-K_α radiations (along with K_β filter) at voltage and current of 40kV and 40mA respectively was used as XRD instrument for recording XRD profiles. Each profile was recorded within the 2θ range from 20° to 80° with scanning rate of 2°/min. Structural arrangement (amorphous/crystalline) of samples (as-prepared and annealed) were analyzed through obtained XRD profiles.

2.2.3 FTIR

FTIR spectroscopy helps to identify presence of functional groups, different structural units and provide their quantitative description. FTIR spectra of as-prepared glass samples were recorded through Perkin Elmer Frontier FTIR Spectrometer using KBr pellet technique. In KBr pellet technique, both sample powder and KBr were mixed homogenously in ~1:100. This mixture was put in 13mm radius die-set (dia. ~ 13mm) and then hydraulically pressed in order to get an almost transparent pellet. Spectral modifications such as baseline and noise corrections were performed using Spectrum 10 analysis software (available with instrument).

2.2.4 Dielectric analysis

A thin layer of colloidal silver paint was pasted at both ends (which helps to improve connectivity and act as electrodes) of rectangular shaped polished sample. The dielectric analysis was performed using impedance analyzer (model: HIOKI IM 3570) operating within frequency range from 1 kHz to 10^6 Hz and temperature range from ambient temperature to 450 °C with heating rate of 1 °C/min. Series capacitance (Cs), parallel capacitance (Cp), impedance (Z) and series resistance (Rs) were fetched from analyzer through external triggering at each temperature with a gap of 5 °C throughout the mentioned frequency range. The formulas used for calculation of dielectric parameters are listed below:

$$\varepsilon' = C_p t/(\varepsilon_\circ A) \qquad \text{(iii)}$$

$$tan\delta = \frac{\varepsilon''}{\varepsilon'} \qquad \text{(iv)}$$

$$\sigma_{ac} = 2\Pi f \varepsilon_\circ \varepsilon' tan\delta \qquad \text{(v)}$$

Where ε' is real and ε'' is imaginary component of dielectric constant (ε), ε_o is absolute dielectric permittivity, A, t, f, $tan\delta$ and σ_{ac} are area of cross-section, thickness of sample, frequency applied, loss tangent and ac conductivity respectively.

2.2.5 UV-Visible absorption

Optical behaviour of as-prepared glass samples was analyzed through UV-Vis NIR spectroscopy. UV-Vis absorption spectra (or optical absorption spectra) were performed at room temperature (for both as-prepared and annealed glasses) using Perkin Elmer LAMDA 750 UV-Vis NIR spectrophotometer, with wavelength range of operation from 300 nm to 900 nm at room temperature.

2.2.6 Differential Thermal Analysis (DTA)

The thermal behavioural analysis for as-prepared glass samples were analyzed using DTA thermograms. These thermograms were recorded using DTA simultaneous measuring instrument (model: DTG 60 H) in temperature ranging from 300°C to 600°C at a heating rate of 10°C/min.

3. Result and Discussion

3.1 Density measurements

Density measurement is a crucial intensive property of glasses as it helps to identify any structural change inside the glass matrix because of compositional alterations. Density of glass systems is generally controlled by various factors like ionic radii, size, mass of modifier and concentration of non-bridging oxygen inside glass matrix [15,38–40]. Table 1 contains measured density values and calculated molar volume values for as-prepared glass samples. Density values for present glass samples were found to lies around 5.5 g/cc to 6 g/cc. In general, addition of Nb_2O_5 with replacement of V_2O_5 is expected to provide an increase in density (due to increasing molar mass of composition) and thereby enhance the compactness of glass network. As expected, we have observed an increasing trend in density with enhanced Nb_2O_5 substitution.

Oxygen packing density (*OPD*) helps to analyze structural compactness of glass matrix (i.e. how tightly oxygen atoms are assigned). *OPD* for all as-prepared glass samples was calculated as per literature [40,41] and obtained values are reported in Table 1. During all compositions total number of oxygen atoms per formula unit remains invariant, which leads to almost similar values of *OPD* for as-prepared glass samples. Along with this, *OPD* can also be related to N_4 (concentration of four coordinated boron atoms) directly (i.e. the increase in N_4 leads decreases in V_m and increase in OPD) [42]. On behalf of increasing density, OPD values and decreasing molar volume, one can suggest that replacement of Nb_2O_5 in place of V_2O_5 causes strengthening of bonds present inside the glass matrix.

3.2 X-ray Diffraction (XRD)

XRD profile helps to analyze the structural arrangement of constituents in glass/glass ceramic network. Figures 1(a & b) shows X-ray Diffraction profiles of NVBBB (as-prepared and annealed) glass system. In Figure 1(a), appearance of a broad hump in diffraction pattern of each glass shows amorphous nature of all as-prepared glass samples (although, some nano-crystalline nucleating agents may be present with short range ordered structure) [33].

As-prepared glass samples were exposed thermally (annealed at ***450℃ for 5 hours),*** in order to identify any sort of crystalline phase growth inside the glass matrix on account of thermal induction (due to nucleation and growth processes) [43–45]. The availability of crystalline seeds with short range ordered structure led to the formation of crystalline phase in glass matrix which is evident through sharp peaks in obtained diffraction patterns (Figure 1(b)). These XRD profiles were analyzed by matching with JCPDS data and it was found that this diffraction data matches with crystallite phase of $Bi_{45}BO_{69}$ (JCPDS card number 42-0294). The size of crystallites developed inside the annealed glass matrix corresponding to the most intense peak (201) was calculated using Debye-Scherrer equation [18,46]. The XRD profile of annealed glass samples matches the diffraction profile of crystallite phase with chemical formula **$Bi_{45}BO_{69}$** (having JCPDS card number 42-0294). Other structural parameters such as lattice parameters (a,b,c), inter-planer spacing (d), calculated volume (V_{cal}), given volume (V_{given}) and lattice strain were also estimated and obtained values are reported in Table 2. A close analysis of data available in Table 2

concludes that nano-crystallites developed inside the glass matrix on annealing at 450 °C for 5 hours fulfil the conditions and criteria for use of these compositions as transparent glass ceramics (TGC).

3.3 Fourier Transform Infrared (FTIR) Spectroscopy

FTIR spectroscopy helps in identification of different structural units that constitute the glass matrix and functional groups in chemical composition of as-prepared glass samples. In order to identify existence of different structural units inside glass matrix, fingerprint region of FTIR spectra was analyzed. The fingerprint region of boro-bismuthate glasses consists of three wide absorption bands (i.e. bands from 1500 to 1100 cm^{-1}, from 1100 to 800 cm^{-1} and 800 to 600 cm^{-1}) corresponding to various bending and stretching vibrations in different structural units. The IR band from 1500 to 1100 cm^{-1} is due to B-O stretching vibrations in BO_3 structural units. With moving towards higher energy, band in 1100 to 800 cm^{-1} and from 800 to 600 cm^{-1} range arise due to stretching vibrations in BO_4 structural units and B-O-B bending vibrations in borate network respectively [27,47–51]. Addition of heavy metal oxides (like BaO and Bi_2O_3) reduces the phonon energy of glass matrix. Figure 2 (a) shows FTIR spectra of as-prepared glass samples recorded using KBr pellet technique at room temperature.

The band lying between 650 to 400 cm^{-1} arises due to various M-O (metal-oxygen) vibrations (such as Ba-O, Bi-O, V-O, etc.) in glass structure [47,49]. Deconvolution on FTIR spectra was used to get a better idea of different bonds or structural units present inside the sample matrix. It helps to identify different peak positions and their corresponding relative peak areas along with NBO concentration constituting the complete spectrum. Deconvolution of recorded FTIR spectrum was performed using '**Gaussian distribution function**' through '**Origin 9.0**' software. Figure 2(b) shows a deconvoluted FTIR spectra of typical NVBBB(x=5) glass sample (here green line shows constituting peaks and red is fitted one). The observed peak centre and their corresponding bands of origin are given in Table 3. On basis of deconvolution one can suggest that glass structure consists of non-bridging oxygen's alongside different structural units listed in Table 3.

Parameter N_4 helps to identify content of non-bridging oxygen inside the sample matrix via relation discussed below.

$$N_4 = \frac{Area\ under\ peaks\ corresponding\ to\ BO_4\ structural\ units}{Sum\ of\ area\ under\ peaks\ corresponding\ to\ BO_4\ \&\ BO_3\ structural\ units} \quad \text{(vi)}$$

Higher content of the BO_4 structural unit lowers the concentration of non-bridging oxygen and molar volume [27,52]. All the structural modification within glass matrix results variation in non-bridging oxygen's (i.e. NBO's) concentration, which can be analyzed by using change in relative area under BO_4 structural units (i.e. N_4). The inset of Figure 2(a) shows compositional variation of N_4 for prepared glass system. N_4 shows increasing trend (with increase in Nb_2O_5 content) for as-prepared glass samples, resulting in compactness of glass matrix as described by compositional trends in density as well.

3.4 Dielectric Analysis

a) Dielectric constant

Dielectric analysis was performed on the basis of dielectric parameters like real component and imaginary component of dielectric constant, a.c. conductivity, loss tangent, etc. Isothermal curves (at temperature = 350 °C) of ε′ (real component) and ε″ (imaginary component) vs frequency for as-prepared glass samples are exposed in Figures 3(a & b), respectively. There are several factors (such as hoping, ionic rotation around negative sites, etc.) that affect the dielectric permittivity of any material. As per figures, the values of ε′ and ε″ decrease with rise in frequency values (for lower frequency values) and attain saturation at higher frequency region. In lower frequency region, both ε′ and ε″ have higher values, which might be due to domination of polarization and space charge accumulation of charge carriers around glass electrode interface, which restrict the further flow of charge carriers.

With rise in frequency, i.e. a faster periodic reversal in direction of applied electric field, space charge accumulation decreases, resulting in a decrease in values of both ε′ and ε″ [5,19,30,34]. Sample with maximum vanadium content (i.e. NVBBB(*x*=0)) have highest value of dielectric constant, which decreases on imparting Nb_2O_5 in place of V_2O_5 (which might be due to mixed transition metal effect (MTE)) [53]. Dielectric properties of glass systems are also affected by the concentration of NBO's present inside their glass matrix. Higher is the concentration of NBO's, more easily will the sample be polarized and greater will be its dielectric behaviour [15,16,54]. Samples having lower value of dielectric constant can be used as appropriate materials for high frequency signal transmission devices. For analyzing effect of heat on dielectric constant, we use typical curves (at different temperatures) of ε′ and ε″ vs frequency for NVBBB(*x*=5) glass sample, as shown in Figures 4 (a & b), respectively. In dispersive region (i.e. region of lower frequency), temperature has a significant effect (due to thermal agitation), which increases space charge polarization, while for higher frequency region, both curves become temperature-independent.

b) Loss tangent (tanδ)

Loss tangent (or dissipation factor) reflects phase difference between applied electric fields and developed electric fields. One can analyze tanδ as ratio of imaginary (ε″) to real (ε′) component of dielectric constant [19,30]. Figure 5(a) shows tanδ vs frequency curves for all as-prepared glass samples at 350 °C. Loss tangent helps to understand energy losses occurring due to various factors such as conduction, relaxation, resonance, etc. In lower frequency region, tanδ has higher value (due to dominance of relaxation phenomena) and its value decreases with increment in frequency [55,56]. Figure 5(b) reflects temperature dependence of tanδ vs frequency curve for typical NVBBB(*x*=5) glass sample. It can clearly be seen that tanδ follows a similar kind of variation as followed by dielectric loss (ε″). With increase in temperature the thermally accelerated charge carriers cause increase in tanδ values in lower frequency region [30]. The similar kind of behavioural variation is followed by all glass samples.

3.5 ac conductivity (σ_{ac})

The ac conductivity helps to understand how well a material can conduct the alternating current. It depends on various factors, such as frequency of applied field, temperature of material, and impurities inside the material. Figures 6(a & b) are used to understand frequency, compositional and temperature effects on ac conductivity. Figure 6(a) reflects ac conductivity (σ_{ac}) vs frequency curve for all as-prepared glass samples at 350 °C. For lower frequency region, σ_{ac} is almost constant due to charge carriers accumulation at glass-electrode interface, which restricts the flow of charge carriers through interface. With increase in frequency (i.e. periodic reversal of electric field), the space charge accumulation reduces, leads to flow of charge carriers and increase in ac conductivity (σ_{ac}). Glass sample with highest content of vanadium possess highest conductivity in comparison with all prepared glasses. Similar kind of pattern were observed among various researchers (i.e. modification of glass matrix with V_2O_5 results increase in ac conductivity due to hopping of charges between V^{4+} /V^{5+} sites) [34]. As shown in the figure, addition of Nb_2O_5 results decrease in σ_{ac} which may be due to heavier mass of niobium ions (in comparison with vanadium ions) and mixed transition metal effect. Glasses possessing lower ac conductivity can be used for high-voltage operating devices. Figure 6(b) shows σ_{ac} vs frequency curves for typical NVBBB(*x*=5) glass sample at different temperatures. All as-prepared glass samples show similar temperature and frequency variations. The increase in temperature cause increase in thermal agitation, which reduces the activation energy of charge carriers and increases ac conductivity.

3.6 UV-Vis Spectroscopy

The optical behaviour of as-prepared and annealed glass samples was analyzed through their UV-Vis absorption spectrum. These absorption spectra help in identification of various optical parameters such as cut-off wavelength ($\lambda_{cut\text{-}off}$), optical band-gap (E_g), Urbach energy (ΔE) and refractive index (n). A typical optical absorption spectra of NVBBB(x=5) glass samples (as-prepared and annealed) are shown in Figure 7(a), which helps in determining cut-off wavelength (i.e. $\lambda_{cut\text{-}off}$).

$\lambda_{cut\text{-}off}$ giving idea about the compactness of glass structure as a decrease in $\lambda_{cut\text{-}off}$ value reflects strengthening of bonds in glass matrix [18,20,57]. Observed values of $\lambda_{cut\text{-}off}$ for all as-prepared and annealed glass samples are reported in Table 4. One can observe from this table that addition of Nb_2O_5 in place of V_2O_5 results in a decrease in $\lambda_{cut\text{-}off}$, reflecting strengthening of bonds and compactness in glass network.

Earlier, was noticed that, the indirect optical band-gap plays significant role in optical behaviour of amorphous solids (like glass) [58]. The value of indirect optical band-gap (E_g) (at r=2 and 3) was recorded at energy intercept of extended part of linearly fitted portion (dash line) of $(\alpha h\upsilon)^{1/2}$ & $(\alpha h\upsilon)^{1/3}$ vs $h\upsilon$ (energy) curve. The graphical representation of these curves for typical NVBBB(x=5) sample are shown in Figure 7 (b) and Figure 8(a) respectively. It was observed that all compositions exhibit similar kind of optical behaviour. The obtained values of E_g (at r=2 and 3) for all as-prepared and annealed glass samples are listed in Table 4**.** As can be seen from this Table 4, substitution of Nb_2O_5 with V_2O_5 enhances the optical band-gap value, which might be due to the strengthening of bonds constituting glass matrix [16,37]. The compositional variation of indirect optical band-gap is found to support the predictions made through compositional trends in density and FTIR absorption spectra [18,49,59]. The increase in values of E_g reflects decreasing concentration of localized states within forbidden energy band-gap [20].

Urbach energy *(ΔE)* helps in identification of extent of defects and localized states inside the glass matrix [57,60]. Increase in network defects leads to an increase in localized states, which provides a relatively shorter energy path to ground state electrons for jumping in conduction band [57,60,61]. Urbach energy for all the prepared glass samples is calculated as per Urbach rule [57,60,61] and calculated values are reported in Table 4. The value of Urbach energy for an glass sample was calculated from inverse of slope of linearly fitted portion in $\ln(\alpha)$ vs $h\upsilon$ curve. A typical graphical representation of $\ln(\alpha)$ vs $h\upsilon$ curve for NVBBB(x=5) sample is shown in Figure 8(b). A decrease in ΔE value after annealing reflects the reduced content of defects present in glass matrix or localized states within forbidden energy band-gap.

a) Refractive Index

Refractive index helps to identify the transparency of annealed glass samples (i.e. annealed glass (glass ceramics) will be called as transparent glass ceramics if they have similar value of refractive index with glass). Refractive indices for any glass sample may effect by various factors such as coordination number of oxide ions, concentration of NBOs, optical basicity, etc. [39,62]. Refractive indices for all the prepared samples (as-prepared and annealed once) were calculated through optical band-gap value (E_g) (for r=2) via relation 'vii' and reported in Table 4.

$$\frac{n^2-1}{n^2+2} = 1 - \sqrt{\frac{E_g}{20}} \qquad \text{(vii)}$$

Addition of Nb_2O_5 to the glass matrix decreases refractive indices for as-prepared glass samples, reflecting a decrease in polarization and NBO's for prepared glass system. The similar values of refractive index for annealed glass samples reflect their transparent nature. On the basis of recorded values of crystallite size and refractive index, we can say that sample NVBBB(x=3) can be treated as useful material for transparent glass ceramics (TGC).

3.7 Differential Thermal Analysis (DTA)

DTA curves help to analyze thermal properties and characteristic temperatures (such as glass transition (T_g), peak (T_c) and onset (T_x) crystallization temperatures) for as-prepared glass samples [20]. Figure 9 contains, graphical representation of DTA curve for typical NVBBB(x=5) as-prepared glass sample. It was observed that all as-prepared glass samples follow similar kind of DTA curves along with their different characteristic temperatures as reported in Table 5. The existence of an endothermic shift in DTA curves for all glass samples reflects the glassy nature of each glass samples. From this table, we can generalize that the addition of Nb_2O_5 to the glass matrix, increases glass transition (T_g), peak crystallization (T_c) temperature and thermal stability. This increase in glass transition temperature reflects enhanced bond strength and compactness of glass network which was also favored by UV-Vis spectroscopy. The existence of exothermic peak reflects nucleation ability of glasses. The decrease in T_c on addition of TMI's suggests their increasing availability as nucleating agents.

4. Conclusion

Barium-boro-bismuthate glasses modified with Nb_2O_5 and V_2O_5 having composition $x$$Nb_2O_5$-(10-$x$)$V_2O_5$-25BaO-30$B_2O_3-35Bi_2O_3$ (where x = 0, 1, 3, 5, 8, 9 & 10 mol%) were prepared via melt-quench technique and abbreviated as NVBBBx (where x = 0, 1, 3, 5, 7, 9 and 10). XRD profiles of as-prepared and annealed glass samples, confirms their amorphous and crystalline nature (along with development of nano-crystallites in annealed glass matrix) respectively. FTIR spectroscopy indicates existence of BO_3, BO_4, BiO_3 and BiO_6, structural units along with non-bridging oxygen's. The optical, electrical and thermal analysis of as-prepared glass samples were analyzed via Uv-Vis, Impedance spectroscopy and Differential Thermal analysis respectively. The lower values of dielectric constant reflect their usability as appropriate materials for high frequency signal transmission devices. The lower value of ac conductivity ($\sigma_{ac} \sim 10^{-5}$ S/m), suggests their availability for high temperature semiconducting devices. $\lambda_{cut\text{-}off}$ of as-prepared glass samples decreases on replacement of V_2O_5 with Nb_2O_5, reflecting strengthening of bonds present inside the glass samples. The optical band-gap of as-prepared glass samples (ranging from 1.13 to 1.92 eV) increases on substitution of Nb_2O_5 in place of V_2O_5. These values reflect, their applicability in various fields such as infrared photo-detectors, thermo-, opto-electronics. The small increase in optical band-gap after annealing reflects a strengthening of bonds within the glass matrix and non-significant change in glass structure after annealing (i.e. crystallites developed are in very small portion). Refractive index values of as-prepared and annealed glass samples reflect that annealed glasses can be treated as transparent glass ceramics, whereas samples NVBBB(x=3) are good transparent ceramic materials among all prepared samples. The sharp exothermic curve in DTA thermogram reflects the nucleating and crystallization abilities of as-prepared glass samples. The decrease in T_c values reflects that transition metal ions present inside the glass matrix act as nucleating agents.

Acknowledgements

The authors express their gratitude to DST Delhi for furnishing experimental support under the FIST Research Grant (Sanction Order No. & Date: SR/FST/PS-1/2018/32). The Central Instrumentation Laboratory (CIL) of Deenbandhu Chhotu Ram University of Science and Technology, Murthal, is acknowledged by the authors for providing FTIR facilities. Author, Vikas Attri, expresses gratitude to UGC, New Delhi, for the financial support granted under JRF Fellowship F. No.-16-9(June 2018)/2019(NET/CSIR).

References:

[1] C.R. Gautam, D. Kumar, O. Parkash, P. Singh, Synthesis, IR, crystallization and dielectric study of (Pb, Sr)TiO 3 borosilicate glass-ceramics, Bull. Mater. Sci. 36 (2013) 461–469. https://doi.org/10.1007/s12034-013-0489-5.

[2] O.I. Sallam, A.M. Madbouly, N.A. Elalaily, F.M. Ezz-Eldin, Physical properties and radiation shielding parameters of bismuth borate glasses doped transition metals, J. Alloys Compd. 843 (2020) 156056. https://doi.org/10.1016/j.jallcom.2020.156056.

[3] H.H. Hegazy, M.S. Al-Buriahi, F. Alresheedi, S. Alraddadi, H. Arslan, H. Algarni, The Effects of TeO2 on Polarizability, Optical Transmission, and Photon/Neutron Attenuation Properties of Boro-Zinc-Tellurite Glasses, J. Inorg. Organomet. Polym. Mater. 31 (2021) 2331–2338. https://doi.org/10.1007/s10904-021-01933-2.

[4] M.S. Al-Buriahi, E.M. Bakhsh, B. Tonguc, S.B. Khan, Mechanical and radiation shielding properties of tellurite glasses doped with ZnO and NiO, Ceram. Int. 46 (2020) 19078–19083. https://doi.org/10.1016/j.ceramint.2020.04.240.

[5] A. Yadav, M.S. Dahiya, P. Narwal, A. Hooda, A. Agarwal, S. Khasa, Electrical characterization of lithium bismuth borate glasses containing cobalt/vanadium ions, Solid State Ionics. 312 (2017) 21–31. https://doi.org/10.1016/j.ssi.2017.10.006.

[6] H. Doweidar, Y.B. Saddeek, FTIR and Ultrasonic Investigations on Modified Bismuth Borate Glasses, J. Non. Cryst. Solids. 355 (2009) 348–354. https://doi.org/10.1016/j.jnoncrysol.2008.12.008.

[7] S. Bhattacharya, H.D. Shashikala, Effect of BaO on thermal and mechanical properties of alkaline earth borosilicate glasses with and without Al2O3, Phys. B Condens. Matter. 571 (2019) 76–86. https://doi.org/10.1016/j.physb.2019.06.065.

[8] Y.-H. Kao, Y. Hu, H. Zheng, J.D. Mackenzie, K. Perry, G. Bourhill, J.W. Perry, Second harmonic generation in transparent barium borate glass-ceramics, J. Non. Cryst. Solids. 167 (1994) 247–254.

[9] P. Bergo, W.M. Pontuschka, J.M. Prison, C.C. Motta, Investigation of some dielectric properties of phosphate glasses doped with iron oxides , by a microwave technique, Measurement. 43 (2010) 210–215. https://doi.org/10.1016/j.measurement.2009.09.007.

[10] V. Bhatia, D. Kumar, H. Singh, N. Kaur, S.M. Rao, A. Kumar, V. Mehta, S.P. Singh, Structural, optical and thermoluminescence properties of newly developed MnKB: Er3+ glass system, J. Non. Cryst. Solids. 543 (2020) 120113. https://doi.org/10.1016/j.jnoncrysol.2020.120113.

[11] M.S. Dahiya, S. Khasa, A. Yadav, A. Agarwal, Appearance of small polaron hopping conduction in iron modified cobalt lithium bismuth borate glasses, AIP Conf. Proc. 1731 (2016) 3–6. https://doi.org/10.1063/1.4947850.

[12] P. Syam Prasad, V. Himamaheswara Rao, M. Mohan Babu, P. Venkateswara Rao, G. Naga Raju, C. Laxmikanth, Spectroscopic investigations of the PbO-MoO3-P2O5:V2O5 glass system, Phys. Chem. Glas. Eur. J. Glas. Sci. Technol. Part B. 56 (2015) 169–174. https://doi.org/10.13036/17533562.56.4.169.

[13] S. Sanghi, A. Sheoran, A. Agarwal, S. Khasa, Conductivity and dielectric relaxation in niobium alkali borate glasses, Phys. B Condens. Matter. 405 (2010) 4919–4924. https://doi.org/10.1016/j.physb.2010.09.032.

[14] A. El-Denglawey, M. Ahmad, K. Aly, Y.B. Saddeek, A. Dahshan, A study of thermal parameters of some alkali boro-bismuthate glasses, J. Mater. Sci. Mater. Electron. 32 (2021) 23614–23623. https://doi.org/10.1007/s10854-021-06850-1.

[15] S. Rani, S. Sanghi, A. Agarwal, S. Khasa, Influence of Nb2O5 on the optical band gap and electrical conductivity of Nb2O5·BaO·B 2O3, IOP Conf. Ser. Mater. Sci. Eng. 2 (2009) 2–6. https://doi.org/10.1088/1757-899X/2/1/012041.

[16] S. Sanghi, S. Rani, A. Agarwal, V. Bhatnagar, Influence of Nb2O5 on the structure, optical and electrical properties of alkaline borate glasses, Mater. Chem. Phys. 120 (2010) 381–386. https://doi.org/10.1016/j.matchemphys.2009.11.016.

[17] N. Gupta, A. Khanna, Glass and anti-glass phase co-existence and structural transitions in bismuth tellurite and bismuth niobium tellurite systems, J. Non. Cryst. Solids. 481 (2018) 594–603. https://doi.org/10.1016/j.jnoncrysol.2017.12.002.

[18] Vikas, M.S. Dahiya, A. Hooda, S. Khasa, Structural analysis of mixed transition metal ion doped barium-boro-bismuthate glass system, J. Mol. Struct. 1264 (2022) 133291. https://doi.org/10.1016/j.molstruc.2022.133291.

[19] V. Attri, S. Khasa, Structural, Electrical and Optical Analysis of Barium Boro-Bismuthate Glass System: Opto-Electronic Devices, ECS Trans. 107 (2022) 10957–10967. https://doi.org/10.1149/10701.10957ecst.

[20] V. Attri, M.S. Dahiya, R. Kumar, A. Hooda, A. Agarwal, S. Khasa, Electrical, optical and high energy radiation shielding study of TMI-doped multi-component glasses, J. Mater. Sci. Mater. Electron. 34 (2023) 1–16. https://doi.org/10.1007/s10854-023-10625-1.

[21] K.S. Shaaban, N. Tamam, H.A. Alghasham, Z.A. Alrowaili, M.S. Al-buriahi, T.E. Ellakwa, Thermal , optical , and radiation shielding capacity of B 2 O 3 -MoO 3 -Li 2 O-Nb 2 O 5 glasses, 37 (2023). https://doi.org/10.1016/j.mtcomm.2023.107325.

[22] G. Upender, M. Prasad, Optik Vibrational , Optical and EPR studies of TeO 2 -Nb 2 O 5 -Al 2 O 3 -V 2 O 5 glass system doped with vanadium, 127 (2016) 10716–10726.

[23] G.S. Murugan, T. Suzuki, Y. Ohishi, Raman spectroscopic studies of quaternary tellurite glasses containing Nb2O5 and Ta2O5, Phys. Chem. Glas. 46 (2005) 359–364.

[24] Anshu, S. Sanghi, A. Agarwal, M. Lather, V. Bhatnagar, S. Khasa, Structural investigations of vanadyl doped Nb2O 5·K2O·B2O3 glasses, IOP Conf. Ser. Mater. Sci. Eng. 2 (2009). https://doi.org/10.1088/1757-899X/2/1/012054.

[25] N. Elkhoshkhany, E. Syala, Detailed study about the thermal behavior and kinetics characterization of an oxyfluoride tellurite glass, J. Non. Cryst. Solids. 486 (2018) 19–26. https://doi.org/10.1016/j.jnoncrysol.2018.02.008.

[26] W. Holand, G.H. Beall, Glass-ceramic technology, Wiley, United Kingdom, 2019.

[27] A. Yadav, M.S. Dahiya, A. Hooda, P. Chand, S. Khasa, Structural influence of mixed transition metal ions on lithium bismuth borate glasses, Solid State Sci. 70 (2017) 54–65. https://doi.org/10.1016/j.solidstatesciences.2017.06.011.

[28] M. Rezvani, B. Eftekhari-Yekta, M. Solati-Hashjin, V.K. Marghussian, Effect of Cr2O3, Fe2O3 and TiO2 nucleants on the crystallization behaviour of SiO 2-Al2O3-CaO-MgO(R2O) glass-ceramics, Ceram. Int. 31 (2005) 75–80. https://doi.org/10.1016/j.ceramint.2004.03.037.

[29] A. Chakrabarti, A.R. Molla, Synthesis of Eu2O3 doped BaO-TiO2-GeO2 based glass-ceramics: Crystallization kinetics, optical and electrical properties, J. Non. Cryst. Solids. 505 (2019) 354–366. https://doi.org/10.1016/j.jnoncrysol.2018.11.002.

[30] M. Malik, S. Dagar, A. Hooda, A. Agarwal, S. Khasa, Effect of magnetic ion, Fe3+ on the structural and dielectric properties of Oxychloro Bismuth Borate Glasses, Solid State Sci. 110 (2020) 106491. https://doi.org/10.1016/j.solidstatesciences.20

20.106491.

[31] D. Holland, A. Mekki, I.A. Gee, C.F. McConville, J.A. Johnson, C.E. Johnson, P. Appleyard, M. Thomas, Structure of sodium iron silicate glass - a multi-technique approach, J. Non. Cryst. Solids. 253 (1999) 192–202. https://doi.org/10.1016/S0022-3093(99)00353-1.

[32] L.S. Rao, M.S. Reddy, M.R. Reddy, N. Veeraiah, Dielectric dispersion in Li2O-MoO3-B2O3 glass system doped with V2O5, J. Alloys Compd. 464 (2008) 472–482. https://doi.org/10.1016/j.jallcom.2007.10.016.

[33] M.S. Dahiya, S. Khasa, A. Agarwal, Structural, Optical and Thermal Properties of Transition Metal Ions Doped Bismuth Borate Glasses, Phys. Chem. Glas. Eur. J. Glas. Sci. Technol. Part B. 57 (2016) 45–52. https://doi.org/10.13036/17533562.57.2.023.

[34] A. Yadav, S. Khasa, A. Hooda, M.S. Dahiya, A. Agarwal, P. Chand, EPR and impedance spectroscopic investigations on lithium bismuth borate glasses containing nickel and vanadium ions, Spectrochim. Acta - Part A Mol. Biomol. Spectrosc. 157 (2016) 129–137. https://doi.org/10.1016/j.saa.2015.12.027.

[35] A. Yadav, S. Khasa, M.S. Dahiya, A. Agarwal, Nano crystalline Bi2(VO5) phases in lithium bismuth borate glasses containing mixed vanadium-nickel oxides, AIP Conf. Proc. 1731 (2016) 5–8. https://doi.org/10.1063/1.4947851.

[36] A. Yadav, S. Khasa, A. Hooda, M.S. Dahiya, A. Agarwal, P. Chand, EPR and impedance spectroscopic investigations on lithium bismuth borate glasses containing nickel and vanadium ions, Spectrochim. Acta Part A Mol. Biomol. Spectrosc. 157 (2016) 129–137. https://doi.org/10.1016/j.saa.2015.12.027.

[37] S. Khasa, M. Dahiya, A. agarwal, Structural Investigations of Lithium Vanadoxide Bismo-Borate Glasses, J. Integr. Sci. Technol. 1 (2013) 44–47. http://www.pubs.iscience.in/journal/index.php/jist/article/view/48.

[38] A. Bajaj, A. Khanna, B. Chen, J.G. Longstaffe, U. Zwanziger, J.W. Zwanziger, Y. Gomez, F. Gonzalez, Structural investigation of bismuth borate glasses and crystalline phases, J. Non. Cryst. Solids. 355 (2009) 45–53. https://doi.org/10.1016/j.jnoncrysol.2008.09.033.

[39] M. Abdel-baki, F.A. Abdel-wahab, A. Radi, F. El-diasty, Factors affecting optical dispersion in borate glass systems, J. Phys. Chem. Solids. 68 (2007) 1457–1470. https://doi.org/10.1016/j.jpcs.2007.03.026.

[40] S. Rada, P. Pascuta, M. Bosca, M. Culea, L. Pop, E. Culea, Structural properties of the boro-bismuthate glasses containing gadolinium ions, Vib. Spectrosc. 48 (2008) 255–258. https://doi.org/10.1016/j.vibspec.2007.12.005.

[41] M.S. Dahiya, Meenakshi, A. Shankar, A. Agarwal, S. Khasa, On the role of ZnO on properties of vitreous bismuth silicates, J. Alloys Compd. 696 (2017) 688–696. https://doi.org/10.1016/j.jallcom.2016.11.285.

[42] M.S. Dahiya, S. Khasa, A. Agarwal, Thermal characterization of novel magnesium oxyhalide bismo-borate glass doped with VO2+ ions, J. Therm. Anal. Calorim. 123 (2016) 457–465. https://doi.org/10.1007/s10973-015-4913-5.

[43] G.A. Sycheva, Crystal Growth and Nucleation in Glasses in the Lithium Silicate System, J. Cryst. Process Technol. 6 (2016) 29–55. https://doi.org/10.4236/jcpt.2016.64004.

[44] R. Casasola, J.M. Rincón, M. Romero, Glass-ceramic glazes for ceramic tiles: A review, J. Mater. Sci. 47 (2012) 553–582. https://doi.org/10.1007/s10853-011-5981-y.

[45] M. Romero, M. Kovacova, J.M. Rincón, Effect of particle size on kinetics crystallization of an iron-rich glass, J. Mater.

Sci. 43 (2008) 4135–4142. https://doi.org/10.1007/s10853-007-2318-y.

[46] S. Dagar, P. Sharma, S. Khasa, Structural refinement and DC conductivity of cobalt doped copper ferrite Structural Refinement and DC Conductivity of Cobalt Doped Copper Ferrite, 030132 (2020) 0–4.

[47] S. Khasa, M.S. Dahiya, A. Agarwal, FTIR studies of some vanadyl ion doped calcium oxychloride borate glasses, AIP Conf. Proc. 1536 (2013) 671–672. https://doi.org/10.1063/1.4810405.

[48] M.S. Dahiya, S. Khasa, A. Agarwal, Physical, thermal, structural and optical absorption studies of vanadyl doped magnesium oxy-chloride bismo-borate glasses, J. Asian Ceram. Soc. 3 (2015) 206–211. https://doi.org/10.1016/j.jascer.2015.02.006.

[49] A. Yadav, S. Khasa, M.S. Dahiya, S. Dalal, A. Hooda, A. Agarwal, Synthesis, thermal and spectroscopic characterization of lithium bismuth borate glasses containing mixed transition metal ions, Phys. Chem. Glas. Eur. J. Glas. Sci. Technol. Part B. 57 (2016) 146–152. https://doi.org/10.13036/17533562.57.3.018.

[50] P. Narwal, M.S. Dahiya, A. Yadav, A. Hooda, A. Agarwal, S. Khasa, Dy3+ doped LiCl–CaO–Bi2O3–B2O3 glasses for WLED applications, Ceram. Int. 43 (2017) 11132–11141. https://doi.org/10.1016/j.ceramint.2017.05.160.

[51] S. Khasa, M.S. Dahiya, A. Agarwal, P. Chand, EPR , FTIR , Thermal and Electrical Properties of VO 2 + doped BaCl2.BaO.B2O3 Glasses, J. Mol. Struct. 1079 (2015) 15–20. https://doi.org/10.1016/j.molstruc.2014.09.012.

[52] P. Narwal, M.S. Dahiya, A. Yadav, A. Hooda, A. Agarwal, S. Khasa, Improved white light emission in Dy3+ doped LiF–CaO–Bi2O3–B2O3 glasses, J. Non. Cryst. Solids. 498 (2018) 470–479. https://doi.org/10.1016/j.jnoncrysol.2018.01.042.

[53] B. Dutta, N.A. Fahmy, I.L. Pegg, Effect of mixed transition-metal ions in glasses . Part III : The P 2 O 5 – V 2 O 5 – MnO system, 352 (2006) 2100–2108. https://doi.org/10.1016/j.jnoncrysol.2006.02.043.

[54] F.A. Abdel-Wahab, A.M. Fayad, M.Abdel-Baki, H. Abdel-Maksoud, Role of non-bridging oxygen defect in the ionic conductivity and associated oxygen trap centers in lead-borate oxide glass: Effect of structural substitution of PbO for Ag2O and Li2O modifier, J. Non. Cryst. Solids. 500 (2018) 84–91. https://doi.org/10.1016/j.jnoncrysol.2018.06.033.

[55] A.S. Hassanien, I. Sharma, Dielectric properties, Optoelectrical parameters and electronic polarizability of thermally evaporated a-Pb-Se-Ge thin films, Phys. B Condens. Matter. 622 (2021) 413330. https://doi.org/10.1016/j.physb.2021.413330.

[56] A.S. Hassanien, Studies on dielectric properties, opto-electrical parameters and electronic polarizability of thermally evaporated amorphous Cd50S50-xSex thin films, J. Alloys Compd. 671 (2016) 566–578. https://doi.org/10.1016/j.jallcom.2016.02.126.

[57] M.S. Dahiya, A. Yadav, N. Manyani, S. Chahal, A. Hooda, A. Agarwal, S. Khasa, Fe-substituted Co-Li bismuth borate glasses: Crystallization kinetics and optical absorption, J. Therm. Anal. Calorim. 126 (2016) 1191–1199. https://doi.org/10.1007/s10973-016-5622-4.

[58] M.S. Dahiya, A. Agarwal, S. Khasa, Compositional Dependence of Optical Absorption in Barium Oxychloride Borate Glasses, J. Adv. Phys. 6 (2016) 116–120. https://doi.org/10.1166/jap.2017.1302.

[59] S. Thakur, V. Thakur, A. Kaur, L. Singh, Structural, Optical and Thermal Properties of Nickel Doped Bismuth Borate

Glasses, J. Non. Cryst. Solids. 512 (2019) 60–71. https://doi.org/10.1016/j.jnoncrysol.2019.02.012.

[60] J.I. Pankove, Optical Processes in Semiconductors, Dover Publications, New York, 1975.

[61] M. Elahi, D. Souri, Study of optical absorption and optical band gap determination of thin amorphous TeO2-V2O5-MoO3 blown films, Indian J. Pure Appl. Phys. 44 (2006) 468–472.

[62] E.S. Yousef, B. Al-Qaisi, UV Spectroscopy, Refractive Indices and Elastic Properties of the (76-x)TeO2.9P2O5.15ZnO.xLiNbO3 Glass, Solid State Sci. 19 (2013) 6–11. https://doi.org/10.1016/j.solidstatesciences.2013.01.014.

[63] P. Pascuta, M. Bosca, S. Rada, M. Culea, I. Bratu, E. Culea, FTIR spectroscopic study of Gd2O3-Bi 2O3-B2O3 glasses, J. Optoelectron. Adv. Mater. 10 (2008) 2416–2419.

[64] Y.B. Saddeek, K.A. Aly, K.S. Shaaban, A.M. Ali, M.M. Alqhtani, A.M. Alshehri, M.A. Sayed, E.A. Abdel Wahab, Physical properties of B2O3–TeO2–Bi2O3 glass system, J. Non. Cryst. Solids. 498 (2018) 82–88. https://doi.org/10.1016/j.jnoncrysol.2018.06.002.

[65] V. Dimitrov, Y. Dimitriev, A. Montenero, IR spectra and structure of VzO5-GeOe-Bi203 glasses, J. Non. Cryst. Solids. 180 (1994) 51–57. https://doi.org/10.1016/0022-3093(94)90396-4.

[66] I. Ardelean, S. Cora, D. Rusu, EPR and FT-IR spectroscopic studies of Bi2O3- B 2O3-CuO glasses, Phys. B Condens. Matter. 403 (2008) 3682–3685. https://doi.org/10.1016/j.physb.2008.06.016.

Figures

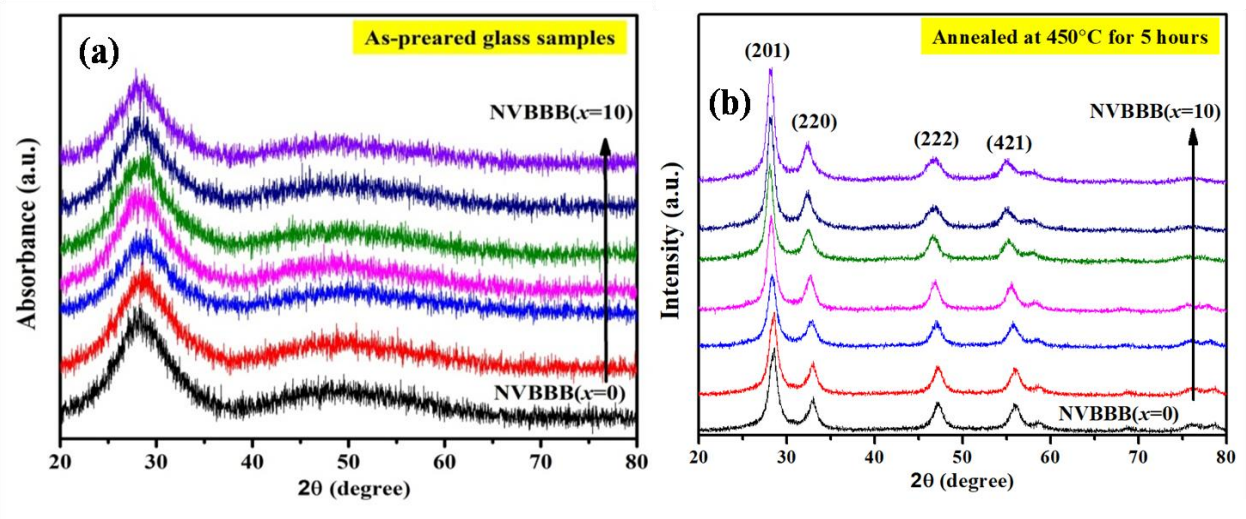

Figure 1. XRD profiles of NVBBB glass system (a) for as-prepared; (b) annealed ones

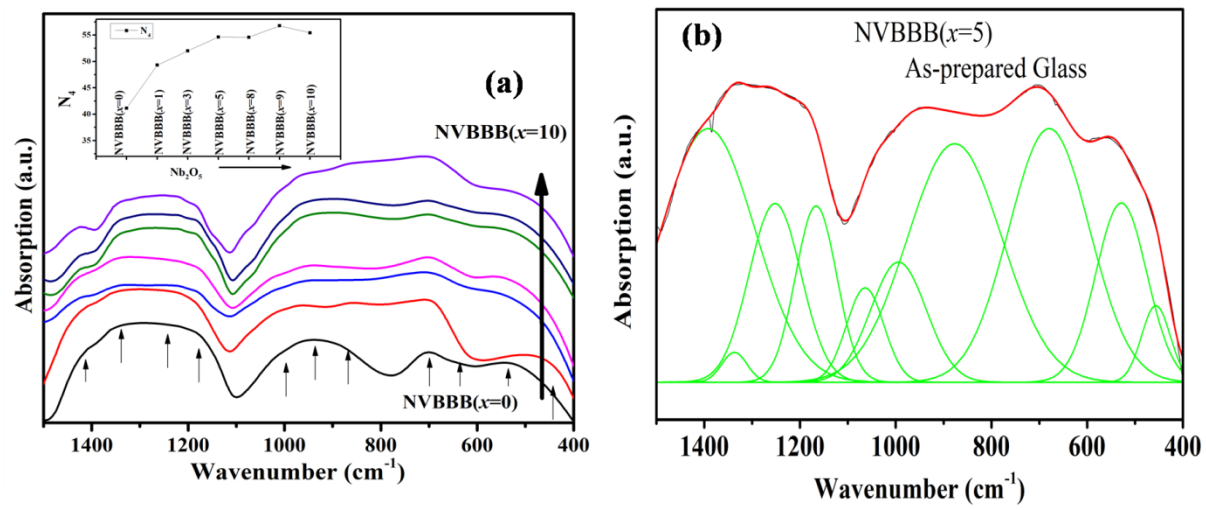

Figure 2. (a) FTIR spectra for all NVBBB glass systems (inset shows N_4 variation for all glasses),

(b) A deconvoluted FTIR spectrum of typical NVBBB(x=5) as-prepared glass sample.

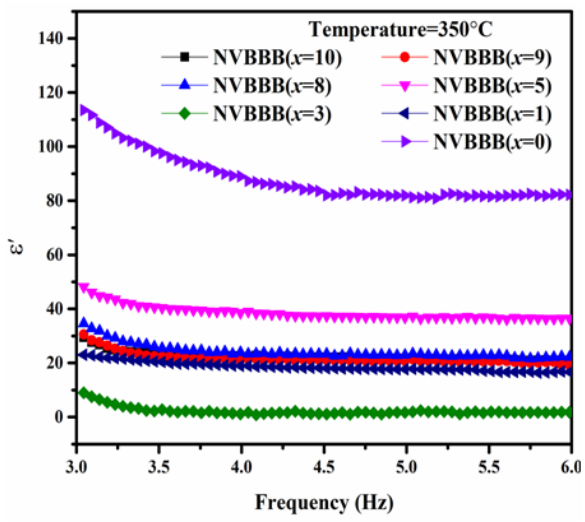

Figure 3. (a) ε′ vs frequency curve for as-prepared NVBBB glass samples at 350°C.

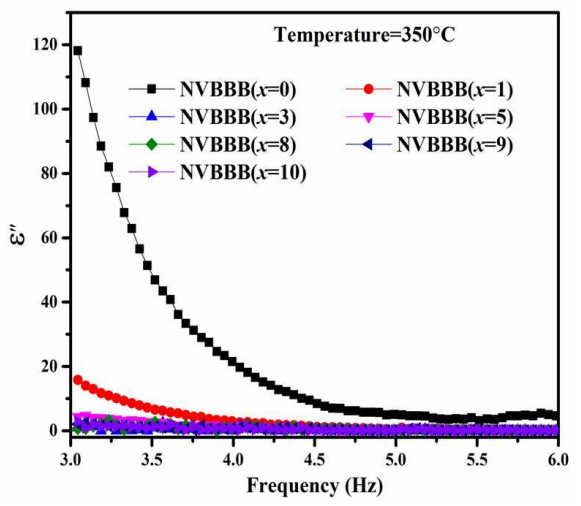

Figure 3 (b) ε″ vs frequency curve for NVBBB glass samples at 350 °C.

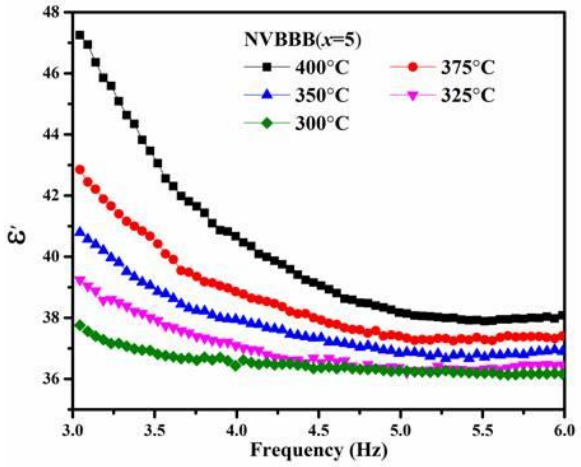

Figure 4. (a) ε′ vs frequency for NVBBB(*x*=5) glass sample at different temperatures

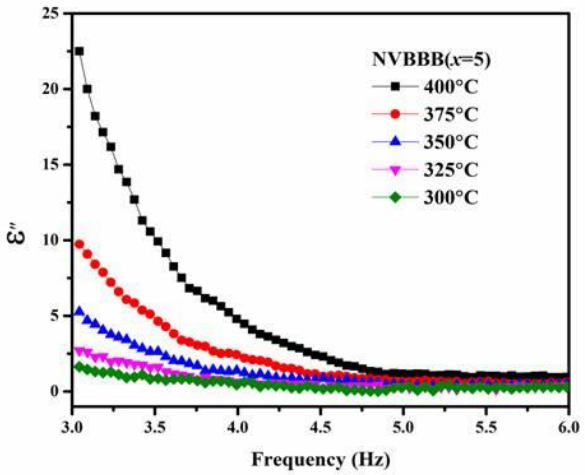

Figure 4. (b) ε″ vs frequency curve for NVBBB(*x*=5) glass sample at different temperatures.

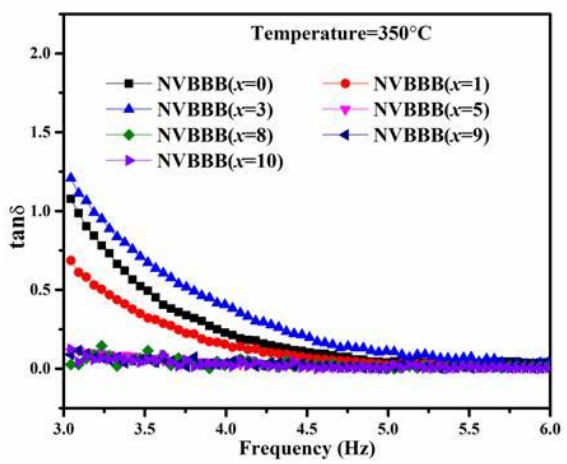

Figure 5. (a) tanδ vs frequency curves for NVBBB glass samples at 350°C

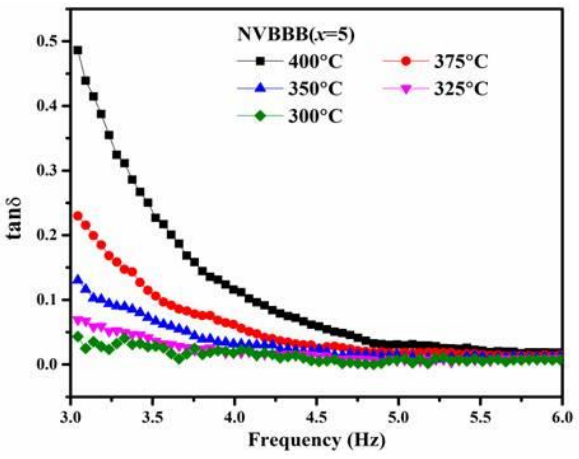

Figure 5. (b) Temperature dependence of tanδ vs frequency curve for NVBBB(x=5) glass sample

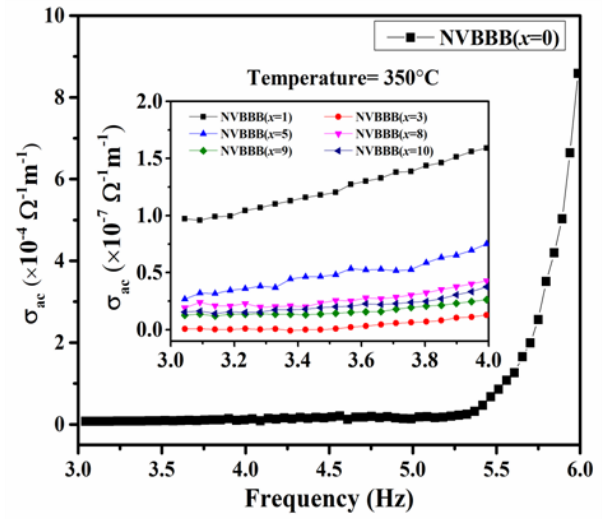

Figure 6. (a) σ_{ac} vs frequency curves for NVBBB glass system at 350°C

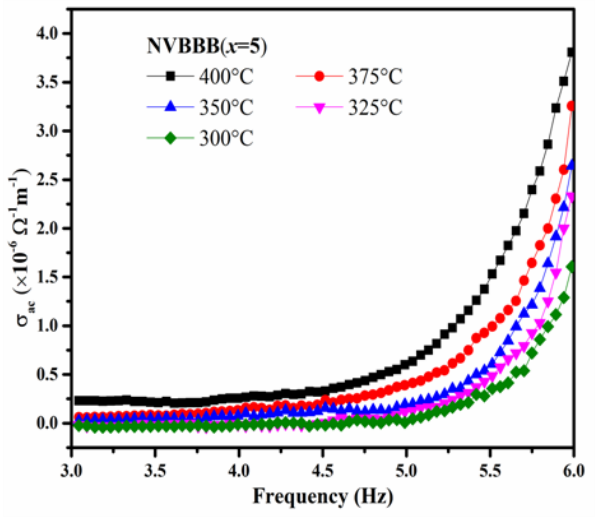

Figure 6. (b) Temperature dependence of σ_{ac} vs frequency curve for NVBBB(x=5) glass sample

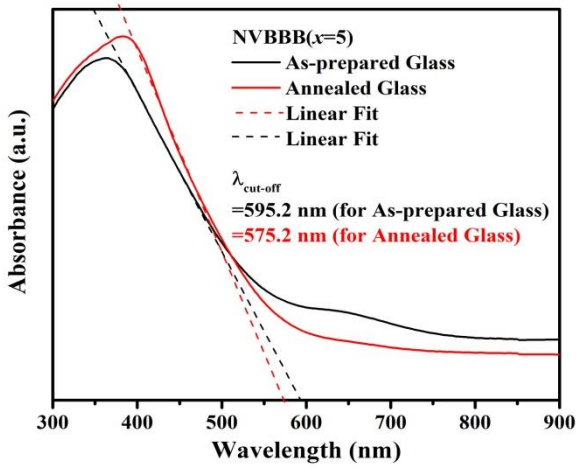

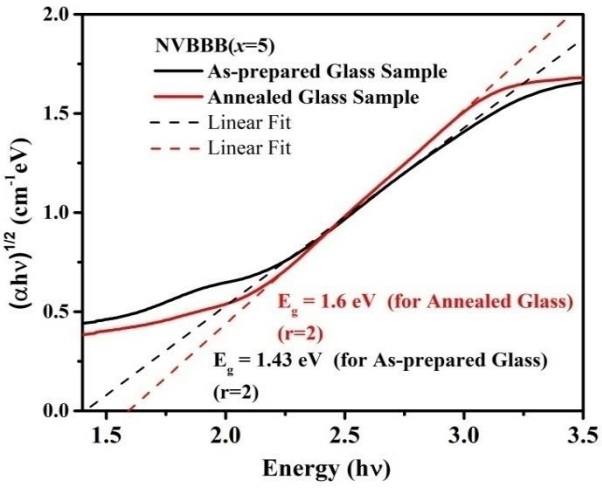

Figure 7. (a) A typical absorption spectra for NVBBB(x=5) as-prepared and annealed glass sample

Figure 7. (b) A typical $(\alpha h\nu)^{1/2}$ vs energy curves for NVBBB(x=5) as-prepared and annealed glass samples at room temperature

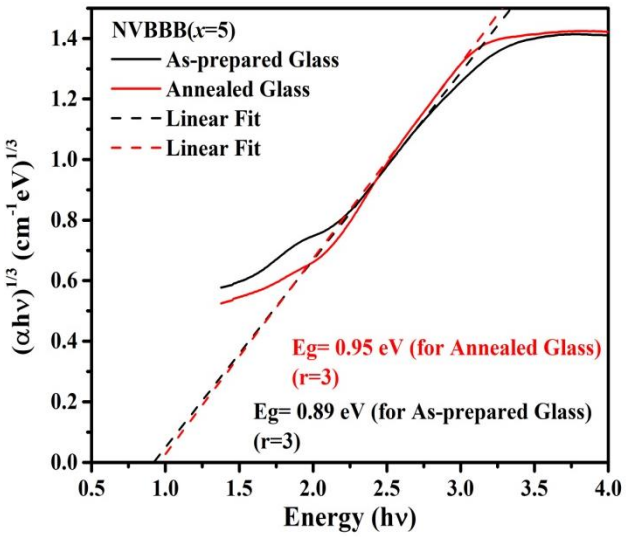

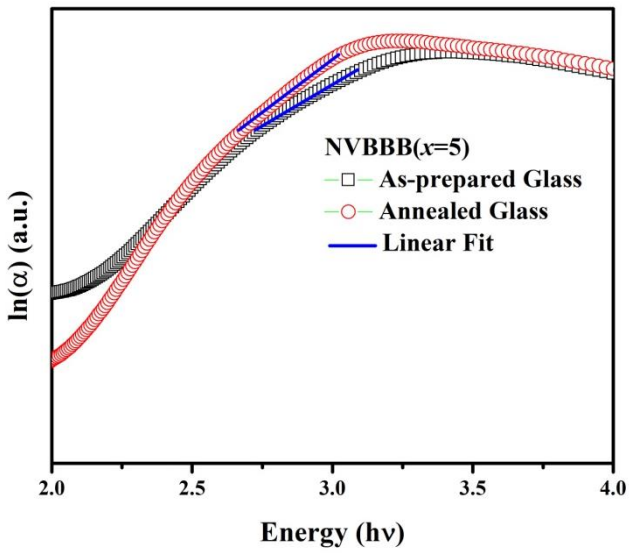

Figure 8. (a) A typical $(\alpha h\upsilon)^{1/3}$ vs Energy ($h\upsilon$) curve for NVBBB(x=5) as-prepared and annealed glass sample

Figure 8. (b) A typical ln(α) vs Energy ($h\upsilon$) curve for NVBBB(x=5) as-prepared glass sample

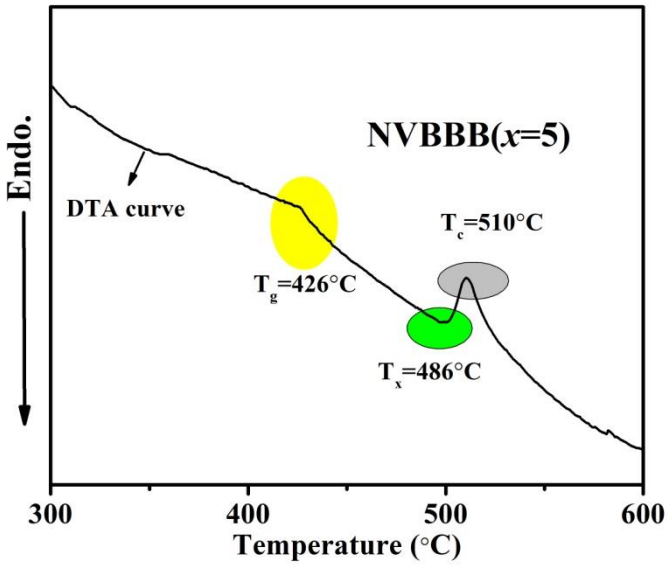

Figure 9. DTA curve for NVBBB(x=5) as-prepared glass samples

Tables

Table 1: Density (ρ), Molar Volume (V_m), Oxygen Packing Density (OPD) for NVBBB as-prepared glass systems

Sample	ρ (g/cc)	V_m (cm^3)	OPD (cm^{-3})
NVBBB(x=0)	5.50	45.30	59.59
NVBBB(x=1)	5.52	45.29	59.61
NVBBB(x=3)	5.54	45.43	59.43
NVBBB(x=5)	5.64	44.92	60.10
NVBBB(x=8)	5.63	45.44	59.47
NVBBB(x=9)	5.71	44.96	60.10
NVBBB(x=10)	5.69	45.26	59.64

Table 2: Structural parameters like Crystallite size (D), inter planer spacing (d), lattice parameters (a,b,c), Volume calculated ($V_{cal.}$), Volume given (V_{given}) and strain inside developed crystalline phase of NVBBB annealed glass matrix.

Sample Name	D (nm)	d (nm)	$a=b$ (A°)	c (A°)	V_{cal} $(A°)^3$	V_{given} $(A°)^3$	Strain
NVBBB(x=0)	6.83	1.109	3.14	1.58	15.578	336.51	0.953
NVBBB(x=1)	6.82	1.108	3.14	1.56	15.381	336.51	0.954
NVBBB(x=3)	6.64	1.112	3.16	1.57	15.677	336.51	0.953
NVBBB(x=5)	6.28	1.107	3.13	1.57	15.381	336.51	0.954
NVBBB(x=8)	5.58	1.103	3.12	1.56	15.186	336.51	0.955
NVBBB(x=9)	5.59	1.097	3.11	1.55	14.991	336.51	0.955
NVBBB(x=10)	5.59	1.097	3.12	1.55	15.088	336.51	0.955

Table 3: Peak centre and their corresponding band of origin for NVBBB glass system

Peak Centre (Wavenumber (cm^{-1}))	Assignment/ band of origin [Refs.]
~470	Vibrations due to metal cations [27,47–51]
~540	Vibrations in Bi-O bonds in BiO_6 structural units [45–48]
~690	Bending vibrations in B-O-B bonds of Borate network [51,63]
~880	Bi-O stretching vibrations in BiO_3 structural units [64–66]
~970	Stretching vibrations in B-O bonds of BO_4 structural units from tri-, tetra- & penta- borate groups [63]
~1165	Stretching vibrations in B-O bond in BO_3 structural units [47,51,63]
~1350	Asymmetric stretching vibrations in B-O bonds from BO_3 structural units [63,66]

Table 4: Optical parameters such as Cut-off wavelength ($\lambda_{cut\text{-}off}$), indirect optical band-gap (E_g) (for r=2 & 3), Urbach energy (ΔE) and refractive index (n) for NVBBB (as-prepared and annealed) glass samples.

As-prepared Glass Samples					
Sample code	$\lambda_{cut\text{-}off}$ *(nm)*	E_g *(eV) (r=2)*	E_g *(eV) (r=3)*	ΔE *(eV)*	n
NVBBB(*x*=0)	636.3	1.13	0.46	0.69	3.26
NVBBB(*x*=1)	630.2	1.21	0.60	0.84	3.19
NVBBB(*x*=3)	622.0	1.34	0.70	0.72	3.09
NVBBB(*x*=5)	595.2	1.43	0.89	0.67	3.04
NVBBB(*x*=8)	542.5	1.53	0.91	0.75	2.97
NVBBB(*x*=9)	513.7	1.67	1.03	0.74	2.89
NVBBB(*x*=10)	490.5	1.92	1.37	0.68	2.77
Annealed Glass Samples					
NVBBB(*x*=0)	606.3	1.35	0.61	0.37	3.09
NVBBB(*x*=1)	615.3	1.39	0.69	0.38	3.06
NVBBB(*x*=3)	585.5	1.40	0.81	0.46	3.05
NVBBB(*x*=5)	575.2	1.60	0.95	0.46	2.93
NVBBB(*x*=8)	534.5	1.72	1.17	0.52	2.83
NVBBB(*x*=9)	519.5	1.78	1.45	0.53	2.84
NVBBB(*x*=10)	517.5	1.85	1.41	0.56	2.80

Table 5: List of characteristic temperatures like T_g, T_x,and T_c and thermal stability (T_s) for NVBBB glass samples.

Sample Code	T_g *(±2℃)*	T_x *(±2℃)*	T_c *(±2℃)*	T_s *(±2℃)*
NVBBB(*x*=1)	420	480	502	82
NVBBB(*x*=5)	426	486	510	84
NVBBB(*x*=8)	428	497	513	85